



LAWRENCE
LIVERMORE
NATIONAL
LABORATORY

LOW-TEMPERATURE DIFFUSION IN CRYSTALLINE COMPOSITION MODULATED FILMS

A. F. Jankowski

December 17, 2004

134th Annual Meeting of The Metallurgical Society
San Francisco, CA, United States
February 13, 2005 through February 17, 2005

Disclaimer

This document was prepared as an account of work sponsored by an agency of the United States Government. Neither the United States Government nor the University of California nor any of their employees, makes any warranty, express or implied, or assumes any legal liability or responsibility for the accuracy, completeness, or usefulness of any information, apparatus, product, or process disclosed, or represents that its use would not infringe privately owned rights. Reference herein to any specific commercial product, process, or service by trade name, trademark, manufacturer, or otherwise, does not necessarily constitute or imply its endorsement, recommendation, or favoring by the United States Government or the University of California. The views and opinions of authors expressed herein do not necessarily state or reflect those of the United States Government or the University of California, and shall not be used for advertising or product endorsement purposes.

Low-Temperature Diffusion in Crystalline Composition-Modulated Films

Alan F. Jankowski

Lawrence Livermore National Laboratory

P.O. Box 808, Livermore, CA 94550 U.S.A.

Abstract

The diffusivity (\check{D}) in alloy systems at low temperatures is determined using composition-modulated structures. An artificial concentration wave is produced by alternating a deposition of the alloy elements. A quantification of the interdiffusivity coefficient is determined by analyzing the decay of the composition fluctuation, that is, the static concentration wave using Khachatryan's microscopic theory of diffusion. As it's customary to assume that there is a linear relationship between $\ln \check{D}$ and T^{-1} over a wide range of temperature (T), the bulk diffusion coefficient represents the long wavelength approximation of the interdiffusivity. The dependency of interdiffusivity on structure is found in general expressions that account for the specific periodicity and growth orientation of the multilayer structure. The kinetics are quantified by analysis of changes in the composition fluctuation with time at temperature through x-ray scattering measurements. In addition to the examination of single-phase crystalline systems as Cu-Ni and Cr-Ti, the theory is now developed to assess diffusion in two-phase layered systems. Specifically, as in Ni-(Cr,Mo) where a face-centered cubic/body centered cubic combination form a pseudo-epitaxial multilayer.

1. Introduction

The use of composition-modulated materials as multilayer films has been a proven method over the past four decades to examine the interdiffusion in materials, both crystalline and amorphous, at low temperatures.^[1-6] Numerous studies of face-centered cubic (fcc) multilayers have used x-ray diffraction to measure the changes in the composition profile, at both high-angle and grazing incidence, that result from thermal anneal treatments.^[1-3,7] The diffusion kinetics can be quantified, as in this presentation, by analyzing the decay of the nanometer-scaled composition fluctuation using the microscopic theory of diffusion.^[2,3,8-10] In particular, examples of fcc multilayers as sputter deposited Cu/Ni and evaporative deposits of Au/Cu will be reviewed.^[1,7]

The thermodynamic stability of body-centered cubic (bcc) superlattices based on chemical disorder has been proposed for Ti-based binary systems.^[11] Specifically, for multilayer pairs consisting of two monolayers of Ti and two monolayers of either Cr or V, energetic stability is predicted for (111) growth wherein the ordering energy is at a minimum. The relative thermal stability of Ti_2/Cr_2 artificial superlattices is assessed for (110) and (111) growth using sputter-deposited multilayer films.^[12]

The behavior of the Ni-22wt.%Cr-13wt.%Mo corrosion-resistant alloy has been studied extensively at high temperatures where aging effects on the microstructure, e.g. heterogeneous precipitation, are known.^[13-16] Unlike single-phase binary or ternary alloys, Ni/(Cr,Mo) alloy forms a two-phase system when studied as a multilayer structure. A direct assessment of stability at temperatures below 800 K is made possible by measuring the interdiffusion of alternating Ni and Cr-Mo layers. The fcc Ni/bcc (Cr,Mo) combination can be addressed using the microscopic theory which accounts for

both the growth texture of each phase in a single treatment as a pseudo-epitaxial system.^[17] As for the single-phase multilayer systems, the interdiffusivity coefficient (\check{D}_B) of several samples (each of a different composition wavelength) are used to determine the macroscopic diffusion coefficient (\check{D}).^[2,17]

2. Experimental Method

2.1 Multilayer synthesis

Metallic multilayers are synthesized from the gas and liquid phase by various methods including aqueous processes as electro-deposition as well as chemical and physical vapor deposition (PVD) methods. In each synthesis approach, the multilayer is formed by a combination of sequential and alternate exposure of the substrate to an array of deposition sources. In most cases, the deposition sources are stationary requiring shuttered exposure of the source to the substrate (which may be translated). An example of sputtering using planar magnetrons will be reviewed.^[7,12,17] The deposition chamber is evacuated by turbomolecular and/or cryogenic pumping to a base pressure less than 1×10^{-5} Pa. The planar magnetron source consists of an inner and outer magnet in the form of right-circular cylinders which provide the magnetic field to accelerate an ionized inert gas to the target (cathode) held at an elevated electrical potential. Typically, the deposition sources are separated from the substrate at a distance sufficient to minimize the effect of energetic sputtered neutrals upon the interface structure that can induce mixing and phase change.^[18-20] For example, the transition from line-of-sight, energetic sputtered neutrals to diffusive thermal atoms occurs for the parameters used wherein a separation of 10 cm accompanies a working argon gas pressure of 0.7 Pa.^[19] The pure

working gas is flowed through a sublimator (e.g. containing molten-metal salts) to remove any impurity gases (as O₂ and N₂) than can cause undesired reactions at the target surface, in the deposition flux, and/or at the substrate surface. The targets are of sufficient density (e.g. >80% full density for ceramics and >99% for metals) to provide a sputter yield and of high purity (>99.9% to avoid undesired alloy effects). Metals are usually deposited with the magnetrons operated in the dc mode at discharge potentials of 150-400 Volts, as primarily dependent on the field strength of the magnetron. The deposition rates are calibrated to the applied target power using quartz crystal microbalances to provide an in-situ monitored control of the deposition process. Instantaneous deposition rates for the metals range, in general, from $(0.4-5) \times 10^{-3} \text{ nm} \cdot \text{W}^{-1} \cdot \text{sec}^{-1}$. Each layer pair of the A/B multilayer is designed to have a specific integral number (n,m) of atomic planes, i.e. A_n/B_m. For the particular case of the Ni-22wt.%Cr-13wt.%Mo alloy, the Ni/(Cr,Mo) multilayers are prepared using a pure target of Ni (>99.99%) and a composite target comprised of Mo and Cr pieces (>99.9% purity).^[17] To approximate the alloy composition of Ni₂(Cr₂Mo) in the multilayer film, the number of Ni atomic planes to number of Cr₂Mo-alloy atomic planes is deposited at a ratio of 5:3. The multilayer film composition is confirmed using Auger electron spectroscopy with depth profiling.^[12] In addition, energy dispersive spectroscopy is used to determine average bulk composition.^[17] The substrates are selected to provide ease in release of the multilayer coatings as free-standing foils and/or to induce specific epitaxial growth orientations. For example, cleaved muscovite is used to release free-standing 1 μm thick Cu/Ni multilayer foils for physical property testing^[7] and sapphire is shown to induce a (111) bcc growth for 0.2 μm thick Ti/Cr multilayers^[12]. For the case of stationary magnetron sources (of

3.3-7.6 cm diameter), the substrates are sequentially rotated before each source at rates that range from 1-10 rev min⁻¹. The measured substrate temperature is less than 400 K during the deposition process.

2.2 Anneal treatments

Anneal treatments at the appropriate temperature can progressively homogenize the multilayer foils. The multilayer specimens are placed within a quartz tube that rests within a tube furnace. The quartz tube is either evacuated by a turbomolecular pump to a base pressure less than 1×10^{-5} Pa or subjected to a continuous flow of an inert gas as argon while heated from room temperature, at a rate of 10-20 K·min⁻¹. The samples are held at the anneal temperature for a period of time (t) and subsequently cooled to 400 K at a rate greater than 100 K·min⁻¹. For the vacuum anneal treatments, the pressure within the quartz tube is less than 3×10^{-5} Pa as the samples are heated and held at temperature.

2.3 X-ray diffraction characterization

The composition wavelength and amplitude of the crystalline multilayers are characterized with x-ray diffraction using Cu $k\alpha$ radiation. A powder diffractometer equipped with a graphite monochromator is operated in the $\Theta/2\Theta$ mode at both grazing incidence and high-angle. The separation measured between the satellite reflections and the (000) incident beam yields the average composition wavelength, i.e. layer pair spacing $d_{A/B}$ for an A/B multilayer, as corrected for refraction. The method to determine the diffraction peak intensities is standard. Each peak is determined using Gaussian(s) fitted to the background intensity. The intensities at grazing incidence can be modeled using kinematical theory to determine the composition profile, as demonstrated for Au/Ni multilayers.^[21] The high-angle diffraction scans reveal the long-range and short-range

ordering of the multilayer. The Bragg reflections indicate the film texture whereas the satellite peaks of increasing order (i) reflect the composition modulation in the growth direction. The wavelength of the composition fluctuation can also be calculated from the separation of the satellites about the superlattice reflection. Each sample is measured in the as-deposited condition ($t=0$) and after the anneal treatment. For reference, The Bragg reflections indicate the film texture whereas the satellite peaks of increasing order (i) reflect the composition modulation in the growth direction. Standard reference values for the interplanar spacing of specific crystalline orientations are: 0.2087 nm for Cu(111); 0.2034 nm for Ni(111); 0.2040 nm for Cr(110); 0.2225 nm for Mo(110); and 0.2338 nm for β -Ti(110).^[22] Each sample is measured in the as-deposited condition ($t=0$) and after each time interval during the sequential anneal treatments. The separation and intensities of the satellite reflections about the superlattice Bragg reflection, e.g. of Au/Ni multilayers, can be fitted to calculate lattice strain in the growth direction using the dynamical theory of x-ray diffraction.^[23] A detailed analysis can be found elsewhere for both the composition profile and lattice distortions within the Cu/Ni superlattice structures.^[24] A Guinier analysis is routinely applied to calculate the composition profile from the high-angle $\Theta/2\Theta$ scans assuming a sinusoidal composition modulation since homogenization of the composition profile (as a consequence of the anneal treatments) is best fit to a sinusoidal variation.^[25-26]

3. Diffusion Model

A quantification of the interdiffusivity is determined by analyzing the decay of the composition fluctuation (or static concentration wave) using the microscopic theory of

diffusion.^[8-10] The advantage of the discrete theory in comparison to the continuous theory is that it can be applied to describe ordering, spinodal decomposition, and artificially introduced composition modulation in disordered solutions where the behavior at short wavelengths is of interest. The satellite peaks about superlattice reflections arise as a consequence of the difference in scattering intensity that results from the composition modulation in the film growth direction. An asymmetry in the satellite spectrum is the result of widely different scattering factors and atom sizes of the modulated solid solution.^[27] In a symmetric case, the component layers have nearly equivalent scattering factors, densities, and atomic weights.^[2,7,22] For example, the intensity of the satellites for the Ni/(Cr,Mo) multilayer samples should be approximately symmetric.^[17]

The peak intensity of the satellite $I^i(t)$ for each order (i) of reflection is normalized to the Bragg reflection $I^B(t)$. The decrease in $I^i(t)$ for the annealed samples from the as-deposited condition of $I^i(0)$ indicates a progressive homogenization of the composition fluctuation with time (t).^[2,8,10] The satellite intensities are proportional to the square of the composition profile amplitude. The relative decay in satellite intensity determines the amplification factor $R(k)$, as previously reported^[8-10], according to the expression

$$\ln\{I^i(t) \cdot [I^i(0)]^{-1}\} = 2R(k) \cdot t. \quad (1)$$

Typically, the decay of the first-order satellites about the Bragg reflection (that is, $i = \pm 1$) are used in the computation of the amplification factor $R(k)$.^[2-3] The $R(k)$ is related to the generalized interdiffusivity (\check{D}_B) through the dispersion relationship $B^2(k)$ as^[10]

$$R(k) = -B^2(k) \cdot \check{D}_B. \quad (2)$$

The dispersion relationship $B^2(h)$ for face-centered-cubic (fcc) growth along the [100] or [111] is given by^[10]

$$B^2(h) = 2 \{1 - \cos(2\pi h)\} \cdot d_{(hkl)}^{-2} \quad (3)$$

where $d_{(hkl)}$ is the (hkl) interplanar spacing of the Bragg reflection,

$$h = d_{(hkl)} \cdot (d_{A/B})^{-1}, \quad (4)$$

and

$$d_{A/B} = 2\pi \cdot k^{-1}. \quad (5)$$

Similarly, derivation of the dispersion relationship $B^2(h)$ for body-centered-cubic (bcc) growth along the [100] or [110] is again expressed by eqn. (3). However, for [111] bcc growth the dispersion relationship is given by^[10]

$$B^2(h) = 2 \{1 - \cos^3(2\pi h)\} \cdot \{3d_{(hkl)}^2\}^{-1} \quad (6)$$

The structural dependency of the $\check{D}_B(s)$ is seen in the dispersion relationship that accounts for the multilayer periodicity and growth orientation.

The bulk diffusion coefficient (\check{D}) can be derived from the interdiffusivity coefficient(s) (\check{D}_B). Typically, the bulk diffusion coefficient (\check{D}) is measured using a macroscopic diffusion couple. It's customary to assume that there is a linear relationship between $\ln \check{D}$ and T^{-1} over a wide range of temperatures. The bulk diffusion coefficient (\check{D}) represents the long wavelength approximation of the interdiffusivity coefficient \check{D}_B . A curvilinear fit to the variation of the interdiffusivity coefficient \check{D}_B with the dispersion relationship $B^2(h)$ yields the bulk diffusion coefficient at $B^2(h)$ equal to zero. That is, a

multilayer with an infinite composition wavelength is the equivalent of a macroscopic diffusion couple. Although it may first appear at long repeat periodicities that \check{D}_B will decrease linearly with $B^2(h)$ or perhaps inversely proportional to $B^2(h)$, it has been shown that use of a higher-order polynomial relationship fits the behavior of \check{D}_B with $B^2(h)$.^[2] Only the higher-order polynomial expression can account for the behavior of \check{D}_B with $B^2(h)$ at very short composition wavelengths.^[2-3] Therefore, the diffusion coefficient \check{D} is related to the interdiffusivity coefficient \check{D}_B by the expression^[2-3]

$$\check{D}_B = \check{D} \cdot \{1 + F_e(h) \cdot (f'')^{-1} + 2(f'')^{-1} \cdot \sum [K_\mu \cdot B^{2\mu}(h)]\} \quad (7)$$

where $F_e(h)$ is the Fourier transform of the elastic strain energy of the distorted lattice, f'' is the second derivative with respect to composition of the Helmholtz free energy per unit volume, μ is the order of the polynomial, and K_μ are the gradient-energy coefficients. In the long wavelength approximation, $-B^2(h)$ equals k^2 . Also, f'' and K_μ are identical with those expressions appearing in the continuous theories^[28-30] or the discrete theory^[31]. Thus, eqn. (7) describes a general polynomial behavior for the variation of \check{D}_B with $B^2(h)$ that has a diffusion coefficient defined as \check{D} . An expansion of the series expression given in eqn. (7) yields

$$\check{D}_B = \check{D} \cdot [1 + K'_1 \cdot B^2(h) + K'_2 \cdot B^4(h) + K'_3 \cdot B^6(h) + \dots] \quad (8)$$

where K'_μ equals $2K_\mu \cdot [f'' + F_e(h)]^{-1}$. A plot of \check{D}_B versus $B^2(h)$ fitted with a polynomial curve determines the diffusion coefficient \check{D} .

4. Experimental Results and Analysis

4.1 Diffraction

A near-square composition wave is fitted to the grazing incidence x-ray diffraction scans using the kinematical analysis^[21] for the composition profiles of the sputter deposited samples, e.g. the Cu/Ni multilayers^[24], in the as-deposited condition. A series of x-ray diffraction scans (in Fig. 1) of the 2.1nm Cu₅/Ni₅ multilayer show the satellite reflections about the (111) superlattice reflection. The decrease in the intensity of the satellite reflections for these vacuum-annealed fcc multilayer samples indicates progressive homogenization with time at 673 K, since the satellite intensities are proportional to the square of the composition profile amplitude.^[26] For the bcc multilayer combination Ti/Cr, a (110) texture is evident at the 2Θ position of 41.90° in the high-angle diffraction scans for multilayer samples deposited on amorphous silica with a Cr seed layer.^[12] However, the satellite intensities are too weak to quantify. So, grazing incidence scans are used to track the effect (shown in Fig. 2) of successive anneal treatments at 473 K on the Ti₂/Cr₂ multilayers that decrease the reflected intensity of the first order satellite reflections with time.

The x-ray diffraction scans for the Ni/(Cr,Mo) multilayer samples evidence a fcc(111)/bcc(110) multilayer structure.^[17] The single Bragg reflection at the 2Θ position of 44.10° (in Fig. 3) for the 8.1nm Ni₂₄/(Cr₂Mo)₁₄ multilayer represents a superposition of the reflections for Ni(111) and Cr₂Mo(110). As for the fcc multilayers and the bcc multilayers, the satellite peaks for the Ni₂₄/(Cr₂Mo)₁₄ multilayer show a decrease in intensity with respect to the Bragg reflection with anneal time at 760 K. To confirm this growth mode, transmission electron microscopy of the fcc/bcc multilayer is performed in

plan view. Selected-area diffraction of the $\text{Ni}_{24}/(\text{Cr}_2\text{Mo})_{14}$ multilayer (seen in Fig. 4) show the diffraction rings that are indexed to the component phases of fcc Ni[111] and bcc Cr_2Mo [110]. For example, the measured interplanar spacings of the (hkl) reflections are: 0.205 nm for (110) bcc; 0.146 nm for (002) bcc; 0.126 nm for (220) fcc; and 0.081 nm for (222) bcc. Although composed of two-phases, the diffraction scans in the $\Theta/2\Theta$ mode yield a single Bragg reflection indicative of a pseudo-epitaxial structure.

4.2 Diffusion

A linear decay is evident in the semi-logarithmic plots of the normalized integrated intensity $I^i(t) \cdot [I^i(0)]^{-1}$ of the satellite reflections with anneal time (in Fig. 5) for each multilayer system. Results are plotted for the first-order satellites of the 0.9nm $\text{Ti}_2/\text{Cr}_2(110)$ multilayer at grazing incidence as well as the first-order satellites below the Bragg reflection for the 2.1nm $\text{Cu}_5/\text{Ni}_5(111)$ multilayer. In addition, the results are plotted for first-order satellites below the Bragg reflection of the $\text{Ni}/(\text{Cr}_2\text{Mo})$ multilayers with 3.3nm, 5.0nm, and 8.1nm composition wavelengths. The linear decay with satellite intensity at later times is consistent with the smaller composition fluctuations proposed within the context of the microscopic model. This occurs after an initial and rapid drop in satellite intensity (for short annealing times) that has been attributed to several factors including recrystallization and grain growth that drive the early stages of annealing as well as the nonlinearity of the diffusion equation.^[2,32]

The $R(k)$ value for each linear curve of Fig 5 is determined from eqn. (1) using a linear regression procedure to fit the variation of $\ln\{I^i(t) \cdot [I^i(0)]^{-1}\}$ with time.^[2] The B^2 values for each multilayer are determined using eqn. (3). Again note that eqn. (3) is singularly applicable for fcc(111)/bcc(110) multilayer growth, so that a single value of

$B^2(h)$ is determined for each of the Ni/(Cr₂Mo) multilayers. Next, the \check{D}_B values are next computed using eqn (2). A fit of the \check{D}_B variation with $B^2(h)$, as plotted in Fig. 6 for the Ni/(Cr₂Mo) multilayers, is accomplished using eqn. (7) as represented in the general expansion seen in eqn. (8). A ($\mu=2$) second-order polynomial expansion results in the following expression

$$\check{D}_B = \check{D} \cdot [1 - 0.616B^2(h) + 0.104B^4(h)] \quad (9)$$

The \check{D}_B intercept at $B^2(0)$ yields the bulk \check{D} value of $3.3 \times 10^{-19} \text{ cm}^2 \cdot \text{sec}^{-1}$ for Ni/(Cr₂Mo) at 760 K. Similarly, and for comparison, values of \check{D}_B with $B^2(h)$ are plotted from data reported for the fcc Au/Cu multilayer system at 533 K.^[1] Using the fitting procedure as presented in eqn. (8), the \check{D}_B intercept at $B^2(0)$ yields the bulk \check{D} value of $4.3 \times 10^{-19} \text{ cm}^2 \cdot \text{sec}^{-1}$ for Au/Cu at 533 K. In both cases, a second-order polynomial is needed and used for fitting the \check{D}_B with $B^2(h)$ variation to produce a correlation coefficient greater than 0.96. A higher-order fit is not necessary. A similar but smaller diffusion coefficient \check{D} of $2.4 \times 10^{-20} \text{ cm}^2 \cdot \text{sec}^{-1}$ is computed for Au/Cu from the anneal data reported at a temperature of 498 K.^[1] Likewise, \check{D} values of $4.4 \times 10^{-22} \text{ cm}^2 \cdot \text{sec}^{-1}$ and $1.8 \times 10^{-20} \text{ cm}^2 \cdot \text{sec}^{-1}$ are approximated for Ti/Cr at 473 K and Cu/Ni at 673 K, respectively. The present \check{D} value for Cu/Ni(111) at 673 K is comparable to the $(2-3) \times 10^{-20} \text{ cm}^2 \cdot \text{sec}^{-1}$ range reported for studies of 2nm Cu/Ni(111) multilayers prepared by the thermal evaporation method.^[33] The diffusion coefficient $\check{D}(T)$ at temperature (T) can be described by the general expression

$$\check{D}(T) = D_0 \cdot e^{-(Q/RT)} \quad (10)$$

where Q is the activation energy for diffusion and R is the universal gas constant ($2 \text{ kcal}\cdot\text{mol}^{-1}$). To compare the relative values obtained for the multilayers, the variation of $\ln \check{D}$ with T^{-1} is plotted in Fig. 7 along with high-temperature tracer diffusion data of Cr^{51} in Ni, Cr^{51} in β -Ti, Cu^{64} in Ni, and Au^{198} in Cu.^[34-36]

5. Discussion

The dispersion relationship of eqns. (3) and (6) is applied in a straightforward manner to assess the role of crystalline orientation in analysis of the diffusivity for the single-phase fcc and bcc multilayer systems, as Cu/Ni(111) and Ti/Cr(110). For the fcc/bcc multilayer combination of Ni/(Cr,Mo), the microscopic theory of diffusion is used to treat the pseudo-epitaxial system as a single-phase surrogate since the formalism for the dispersion relationship of eqn. (3) does not differentiate between a (111) fcc and (110) bcc structure. The single Bragg reflection observed in Fig. 3 for the multilayer is consistent with the Ni(111) fcc and $\text{Cr}_2\text{Mo}(110)$ bcc growth variation. The electron diffraction pattern (of Fig. 4) taken in plan view is similar to the Kurdjumov-Sachs growth relationship previously seen for another fcc/bcc multilayer system, i.e. Au/Nb.^[37]

When the high-angle x-ray reflections are not well-defined, as e.g. is the case for amorphous multilayer structures, then the grazing angle satellites can be used to determine the diffusion coefficients.^[4-6] Use of the grazing angle satellites for determining the interdiffusivities \check{D}_B of textured-crystalline multilayer materials may inadvertently omit the crystallographic reference of the short-range order that corresponds with the dispersion relationship $B^2(k)$ and amplification factor $R(k)$ of eqns.

(1) and (2). It may be of future interest to compare the diffusivity obtained at high angle with the value obtained by analysis of the grazing incidence satellites.

A remarkable consistency is observed (in Fig. 7) by interpolation between the high-temperature tracer data and low-temperature multilayer diffusion results. The consistency in this classic Arrhenius behavior of $\ln \check{D}$ vs T^{-1} demonstrates the utility of the multilayer diffusion technique as applied through the microscopic theory of diffusion. This method will next be used to model the thermal stability of a composition gradient in thick Au-Cu coatings.

6. Summary

The decay rate of the short-range order found in crystalline multilayers is measured by the x-ray diffraction and analyzed using the microscopic theory of diffusion^[8-10]. The value for the diffusion coefficient \check{D} is computed for crystalline multilayers as the long wavelength equivalent to a macroscopic diffusion couple. Values of the diffusion coefficient at low temperature are consistent with high-temperature tracer diffusion data for single-phase and pseudo-epitaxial two-phase multilayer systems.

Acknowledgments

This work was performed under the auspices of the United States Department of Energy by the University of California, Lawrence Livermore National Laboratory under contract no. W-7405-Eng-48.

References

1. W.M. Paulson and J.E. Hilliard, *J. Appl. Phys.* **48** (1977) 2117
2. T. Tsakalakos, *Thin Solid Films* **86** (1981) 79
3. A.F. Jankowski and T. Tsakalakos, *Metall. Trans. A* **20** (1989) 357
4. F. Spaepen, *Mater. Sci Eng'g.* **97** (1988) 403
5. F. Spaepen, *J. Magn. Magn. Mater.* **156** (1996) 407
6. W-H.Wang, H.Y. Bai, and W.K. Wang, *J. Appl. Phys.* **86** (1999) 4262
7. A.F. Jankowski, E.M. Sedillo, and J.P. Hayes, *Jpn. J. Appl. Phys.* **33** (1994) 5019
8. A.G. Khachaturyan, *Prog. Mater. Sci.* **22** (1978) 1
9. H.E. Cook, D. de Fontaine and J.E. Hilliard, *Acta Metall.* **17** (1969) 765
10. A.G. Khachaturyan, *Theory of Structural Transformations in Solids*, John Wiley and Sons, New York (1983) pp. 128-136
11. M. Sluiter and P. Turchi, *Phys. Rev. B* **46** (1992) 2565
12. A.F. Jankowski, *NanoStruc. Mater.* **4** (1994) 19
13. R.B. Leonard, *Corrosion* **25** (1969) 222
14. F.G. Hodge, *Corrosion* **29** (1973) 375
15. M. Raghavan, B. Berkowitz, and J. Scanlon, *Metall. Mater. Trans. A* **13** (1982) 979
16. H.M. Tawancy, R.B. Herchenroeder and A.I. Asphahani, *J. Metals* **35** (1983) 37
17. A.F. Jankowski and C.K. Saw, *Scripta Mater.* **51** (2004) 119
18. R.E. Somekh, *J. Vac. Sci. Technol. A* **2** (1984) 1285
19. W.D. Westwood, *Mater. Res. Soc. Bull.* **13**(12) (1988) 46
20. A.F. Jankowski, P. Sandoval, and J.P. Hayes, *NanoStruc. Mater.* **5** (1995) 497
21. J. Chaudhuri, S.M. Alyan and A.F. Jankowski, *Thin Solid Films* **219** (1992) 63

22. B.D. Cullity, Elements of X-Ray Diffraction, Addison-Wesley, Reading, MA (1978)
pp. 512-521
23. J. Chaudhuri, V. Gondhalekar and A.F. Jankowski, J. Appl. Phys. **71** (1992) 3816
24. S. Jayakody, J. Chaudhuri, A.F. Jankowski, J. Mater. Sci. **32** (1977) 2605
25. T. Tsakalakos and J.E. Hilliard, J. Appl. Phys. **54** (1983) 734
26. G.E. Henein and J.E. Hilliard, J. Appl. Phys. **54** (1983) 728
27. S.C. Moss, in Local Atomic Arrangements studied by X-Ray Diffraction, eds. J.B. Cohen and J.E. Hilliard, Gordon and Breach Science, New York, NY (1966) pp. 114-115
28. J.W. Cahn, Acta Metall. **9** (1961) 795
29. J.W. Cahn, Acta Metall. **10** (1962) 179
30. J.W. Cahn and J.E. Hilliard, J. Chem. Phys. **28** (1958) 958
31. H.E. Cook and J.E. Hilliard, J. Appl. Phys. **40** (1969) 2191
32. T. Tsakalakos, Scripta Metall. **20** (1986) 471
33. T. Tsakalakos, Thin Solid Films **86** (1981) 79
34. K. Monma, H. Suto and H. Oikawa, J. Japan Inst. Metals **28** (1964) 188
35. G.B. Gibbs, D. Graham, D.H. Tomlin, Phil. Mag. **8** (1963) 1269
36. A. Chatterjee, D.J. Fabian, Acta Mater. **17** (1969) 1141
37. A.F. Jankowski and P.L. Perry, Thin Solid Films **193/194** (1990) 799

Figures

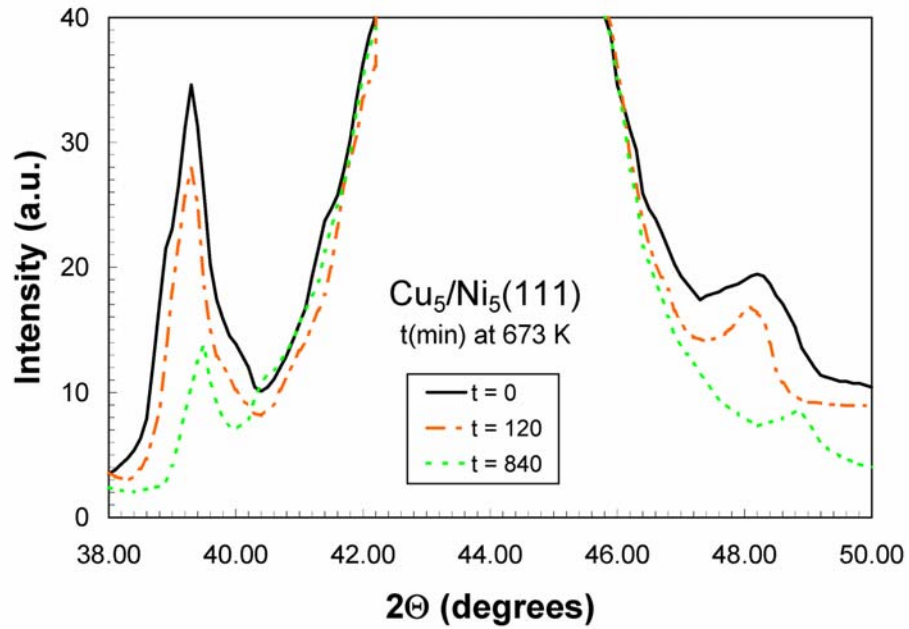


Figure 1. The Cu $k\alpha$ x-ray diffraction patterns taken in the $\Theta/2\Theta$ mode at high angle for the 2.1nm $\text{Cu}_5/\text{Ni}_5(111)$ multilayer sample in the as-deposited ($t=0$) condition and as annealed at 673 K for 120 and 840 minutes.

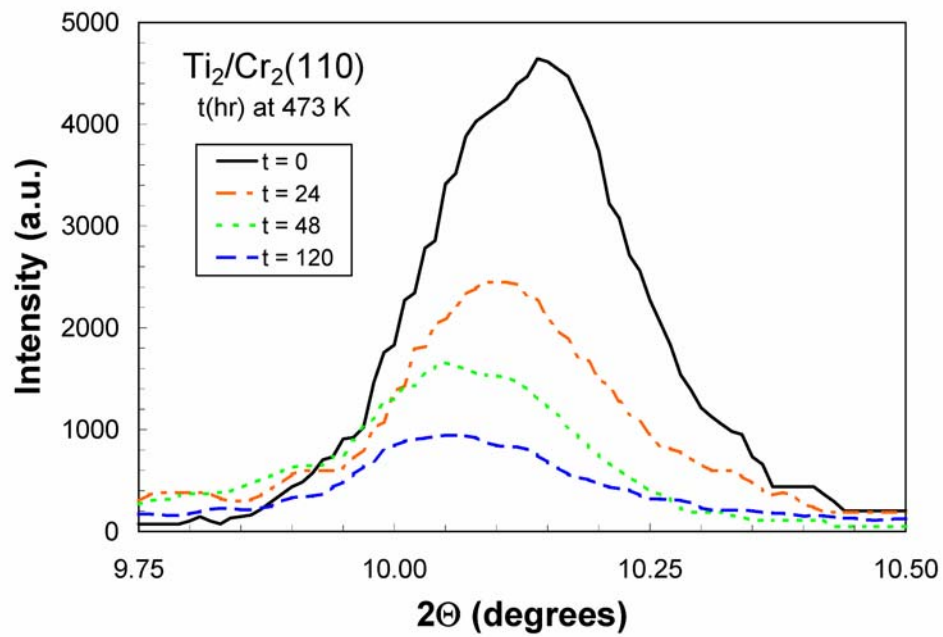


Figure 2. The Cu $k\alpha$ x-ray diffraction patterns taken in the $\Theta/2\Theta$ mode at grazing incidence for the 0.9nm $\text{Ti}_2/\text{Cr}_2(110)$ multilayer sample in the as-deposited ($t=0$) condition and as annealed at 473 K for 24, 48, and 120 minutes.

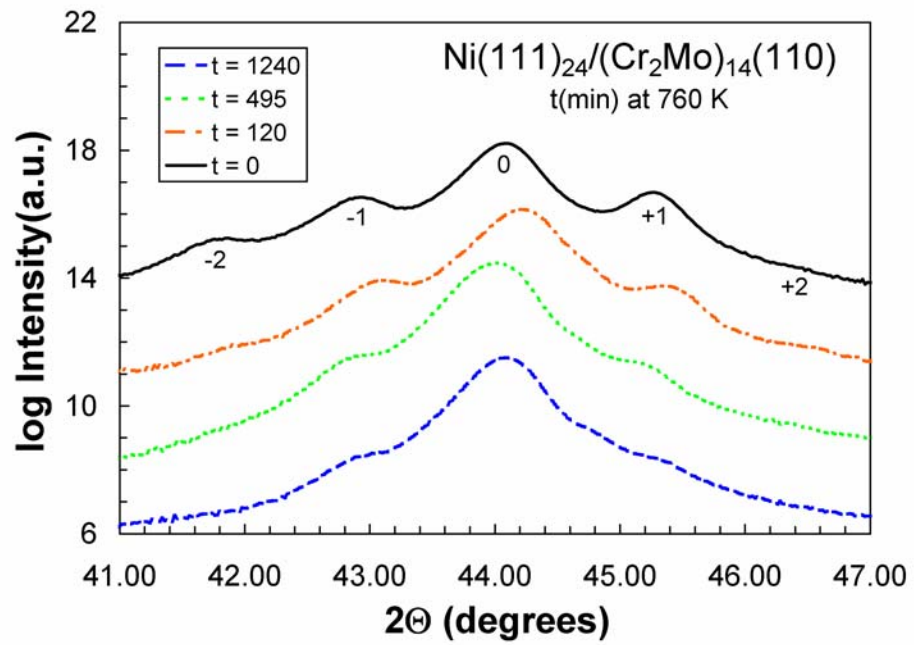


Figure 3. The Cu $k\alpha$ x-ray diffraction patterns taken in the $\Theta/2\Theta$ mode at high angle for the 8.1nm Ni(111)₂₄/(Cr₂Mo)₁₄(110) multilayer sample in the as-deposited ($t=0$) condition and as annealed at 760 K for 120, 495, and 1240 minutes.

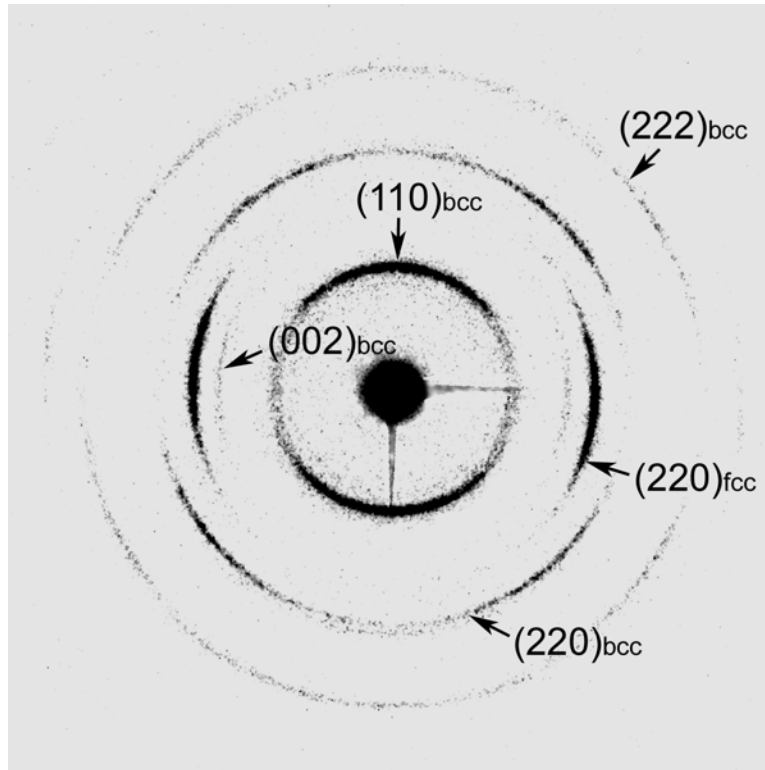


Figure 4. A selected-area diffraction pattern of the 8.1nm Ni(111)₂₄/(Cr₂Mo)₁₄(110) multilayer sample taken in plan view shows the reflections that correspond with a fcc(111) and bcc(110) superlattice growth.

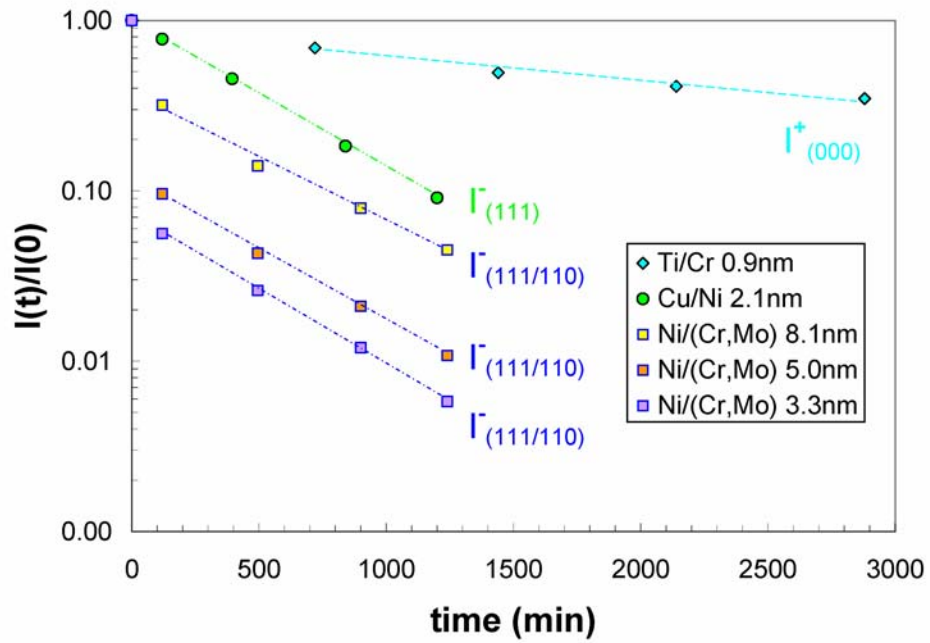


Figure 5. A linear decay with time to the logarithmic variation of normalized satellite intensity occurs for each of the Ti/Cr, Cu/Ni, and Ni/(Cr,Mo) multilayer samples.

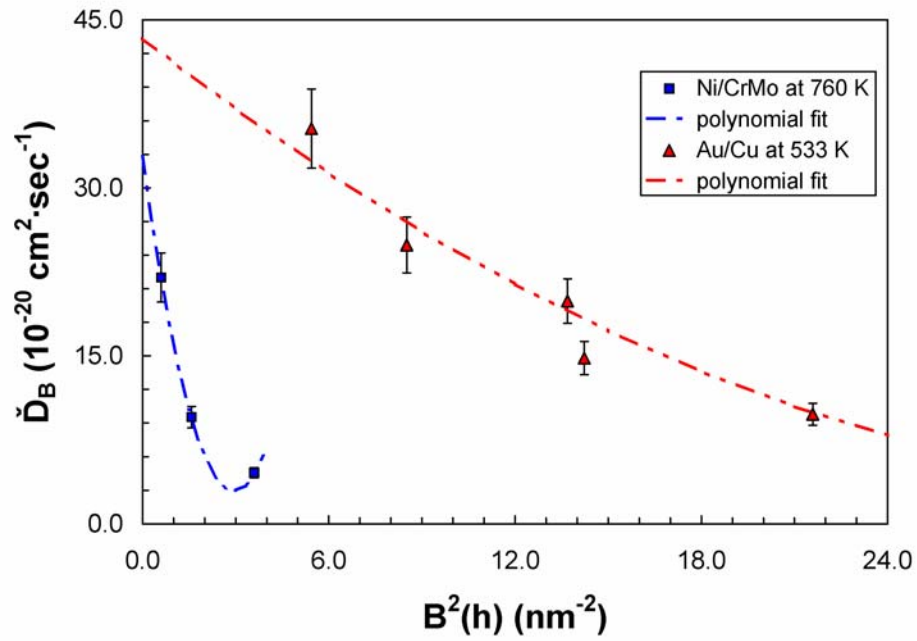


Figure 6. A polynomial fit of the variation of the interdiffusion coefficient \check{D}_B with the dispersion relationship $B^2(h)$, for multilayer samples of Au/Cu annealed at 533 K and Ni/(Cr,Mo) annealed at 760 K, is used to determine the diffusion coefficient \check{D} at $B^2(h) = 0$.

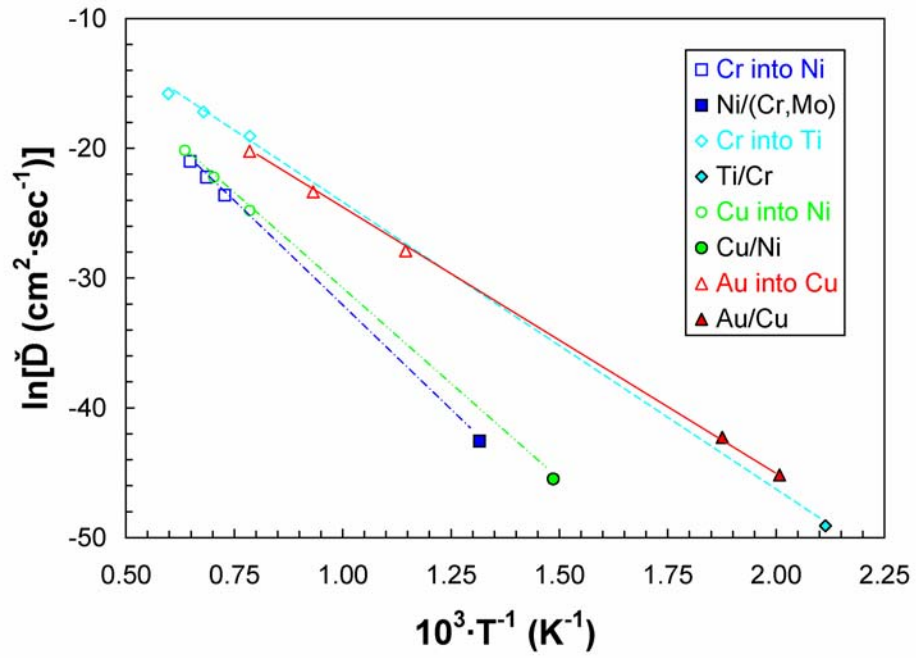


Figure 7. The variation of the diffusion coefficient \dot{D} is plotted at high temperature for tracer isotope diffusion of Cr^{51} in Ni, Cr^{51} in β -Ti, Cu^{64} in Ni, and Au^{198} in Cu along with the low-temperature diffusion results for the multilayers of Ni/(Cr,Mo), Ti/Cr, Cu/Ni, and Au/Cu.